***Original Research Article***

# Numerical simulation and measurement of temperature distribution in water-in-glass evacuated solar water heater

.


## ABSTRACT

**Aims:** This study focused on investigating the thermal behaviour of a water-in-glass evacuated solar heater experimentally and numerically.
**Study design:** The study was carried out in three parts: numerical modelling, experimentation and validation of the numerical modelling results.
**Place and Duration of Study:** The study was carried out in six month at Thermophysics Institute of Northeastern University in Shenyang, China.
**Methodology:** A lab-scale experimental model was developed using two full scale evacuated tubes inclined $45^{o}$ to the vertical and coupled to a rectangular water storage tank. Thermo resistors were connected to multi-channel data logger to record both spatial and temporal temperature distribution of the system. A three-dimensional numerical model was developed using a Computational Fluid Dynamics (CFD) package, Fluent 6.1 to investigate temperature and flow fields. This model interprets exactly the geometry of the lab-scale experimental model so that it can be validated against experimental results. A user defined function was developed to take into account the variation of incident angle with daily and seasonal movement of the sun which affects the amount of heat flux incident on the tube collector.
**Results:** The numerical model showed that flow in the tube is bi-filamental with the hot stream moving up the tube on the top side and the cold stream moving down the tube from the storage tank on the lower side. It also showed that the maximum temperature reached by the water in the system depends upon the amount of incident radiation.
**Conclusion:**The numerical model can be used for predicting temperatures in the water-in-glass solar water heaters.



*Keywords: water-in-glass water heater; Computational Fluid Dynamics, natural flow, conservation equations*


## 1. INTRODUCTION

As a result of climate change and depletion of fossil fuel reserves, many countries are advocating for use of cleaner and renewable sources of energy. This has resulted in great expansion in solar water heating industry. Water-in-glass evacuated tube solar collectors are preferred to other types because they utilize well both beam and diffuse solar radiation. To improve the efficiency of these solar water heaters, researchers need to understand the heat transfer process in both the evacuated tubes and storage tank. Experimentation would be most appropriate to understand the effects of various parameters on heat transfer and long-term performance of evacuated tube solar water heaters but it is too expensive and time consuming. To overcome this barrier, computational fluid dynamics models need be developed for use in the analysis and evaluation of existing systems and find more information for designing new and better systems.

Extensive research has been has been ongoing back dating to 1950s to understand the heat transfer process in evacuated tubes. Martin and Cohen [1] experimentally investigated convective heat transfer in an open thermosyphon tube. They used water, glycerine and air so as to cover a wide range of physical properties of convective fluid. The results suggested that turbulent flow in a closed ended tube is less effective than laminar flow.

Behnia & Morrison investigated free convection flow in an open ended inclined cylindrical thermosyphon with application to an evacuated tubular solar collector [2]. They visualised flow patterns inside the tube using dye and rheoscopic tracer particles and measured temperature using traversing thermocouple rake. The bottom end of the tube was sealed and top end connected to a water reservoir. Water at different temperatures was circulated in heating chambers as heating medium. The tube walls were heated uniformly or differentially where the upper and lower walls were subjected to different temperatures. They observed significant stagnant region, whose length decreased with increasing wall temperature, near the closed end during steady state uniform heating. No stagnation region was observed with differential heating. They also observed natural separation between the inflow and out flow streams. The separation was enhanced by the inclination of the tube. Gaa *et al.* [3] used a similar experimental set up and determined velocity distribution along the central vertical plane at different Rayleigh number, aspect ratio and heating conditions using a laser Doppler anemometer. They performed correlations between axial flow rate and these independent control parameters. They also noticed the bi-filamental flow near the orifice and that differential heating promoted freer flow between the opposing streams even at lower heat input.

Cabanillas *et al.* [4] experimentally measured circumferential distribution of incident radiation on tubular solar collectors using the experimental Device for Measurement of Angular Radiation (EDMAR). The results showed that the radiation distribution on the tube circumference can be represented by a cosine function for the top half while for the lower half the intensity is almost constant.

Morison et *al.* [5] investigated the performance of a water-in-glass evacuated tube solar pre-heater using International Standard test method ISO 9459-2 for a range of locations. They also used a computational fluid dynamics package, Fluent V5.4 to analyse flow through a long single ended thermosyphon inclined at $45^{o}$ to the vertical. Uniform and differential wall heating were used. Stagnation regions were observed near the closed end of the tubes for low Rayleigh numbers and high aspect ratio and this can affect the performance of the collector. They [6]continued their investigations adopting circumferential heat distribution from Cabanillas. A lab scale water heater was developed with a full-scale tube connected to a storage tank. Silicon rubber heaters were used to simulate energy from the sun. Particle Image Velocimetry (PIV) was used to measure flow rate to validate the numerical model. The simulation results showed that flow rate was high enough to disturb stratification in the tank. Both the simulation and experimental results showed that the tank temperature strongly influence the flow rate. Circumferential heat distribution was found to influence the flow structure and rate.

Budihardjo *et al.* [7] carried out numerical and experimental investigations to develop a correlation for natural circulation flow rate through single ended water-in-glass evacuated tubes mounted over a diffuse reflector. Measurements were taken during half hour periods across solar noon on a commercial solar water heater mounted on roof. Circumferential heat distribution was used for heat input boundary condition. They developed a flow rate correlation in terms of solar input, tank temperature, collector inclination and tube aspect ratio. They [8, 9] continued with the investigations. They performed experiments to characterize the system components and developed a numerical model in TRNSYS. The model was used to predict long term performance of water in glass evacuated solar heaters. They compared the performance of water in-in-glass evacuated tube solar heater with flat plate collectors in a range of locations. For Sydney, they found that a 2 panel flat plate collector performed better than a typical 30 tube evacuated tube array.

Kim *et al.*[10] developed a one-dimensional numerical model for a solar system which consists of all-glass solar vacuum tubes. Each tube contained a coaxial fluid conduit in which water is heated as it flows. The water circulation was driven by an external pump. To prevent functional problems as a result of freezing on very cold days, the space between the fluid conduit and glass tube was filled with an antifreeze solution. The model could be used for efficiently designing all-glass solar collector tubes. Han *et al.*[11] investigated the thermal performance of a similar system using a three dimensional model. They assumed that the vacuum received uniform solar radiation regardless of the sun's daily movement. The model could be used to predict spatial variation of water temperature as it flows through the conduit.

Kim and Seo[12] experimentally and numerically investigated thermal performance of a glass evacuated tube considering different shapes of absorber tubes. To obtain realistic results beam and diffuse radiation and shading due to adjacent tubes were taken into account. They observed that the performance of a solar collector is affected by shape of the absorber tube, solar radiation incident angle and the arrangement of collector tubes.

Shah and Furbo [13] developed a prototype collector with parallel-connected evacuated tubes open at both ends utilising solar radiation coming from all directions. They measured the collector performance using an outdoor test facility and developed a theoretical model for the determination of collector's thermal performance. In the model flat plate collector equations are integrated over the whole absorber circumference. The model can be used to predict shading on the evacuated tube as a function of solar azimuth in order to calculate energy from beam radiation correctly. The results showed that for maximum thermal performance, the collector azimuth must be close to the latitude of the location. They [14] went farther to investigate heat transfer and flow structures inside all-glass evacuated tubular collector, with horizontal tubes connected to a vertical manifold, for different operating conditions. For the conditions investigated they observed highest efficiency for the collector with shortest tube length among other things.

Wei *et al.*[15] theoretically studied flat-plate tube-fin and evacuated tube solar collectors with cylindrical absorbers integrated into pitched roof to determine area compensation of non-directly-south facing solar collectors. They considered beam, diffuse and ground reflected radiation contribution to daily energy output from an evacuated tube solar collector. They used MATLAB language for simulations. Basing on their findings they recommended area compensations less than 1.30 for different kinds of solar collectors used in China.

Although much research has been done on heat transfer and performance of evacuated tube solar collectors, nothing has been published on temperature distribution in water-in-glass evacuated tube solar collectors. In these solar water heaters, flow is driven by density variation resulting from temperature difference between water in the tube and that in the tank. When the tube wall is heated, heat is transferred to the adjacent fluid layers which rise thereby drawing the cold water from the tank to replace it as shown in Figure 1.

In the present work the mechanisms of natural convection in evacuated tube solar collectors were investigated. Experimental and numerical models were developed to study the spatial and temporal temperature distribution and flow patterns in the collector tubes and storage tank. The intensity of solar radiation incident on the collector changes depending on the angle of incidence. Since the angle of incidence varies with the daily, from east to west, and seasonal, from north to south, motion of the sun, a UDF was developed to take into account this variation. The ultimate aim of this paper was to validate the numerical model so that it can be used for future studies to predict performance and design optimisation.

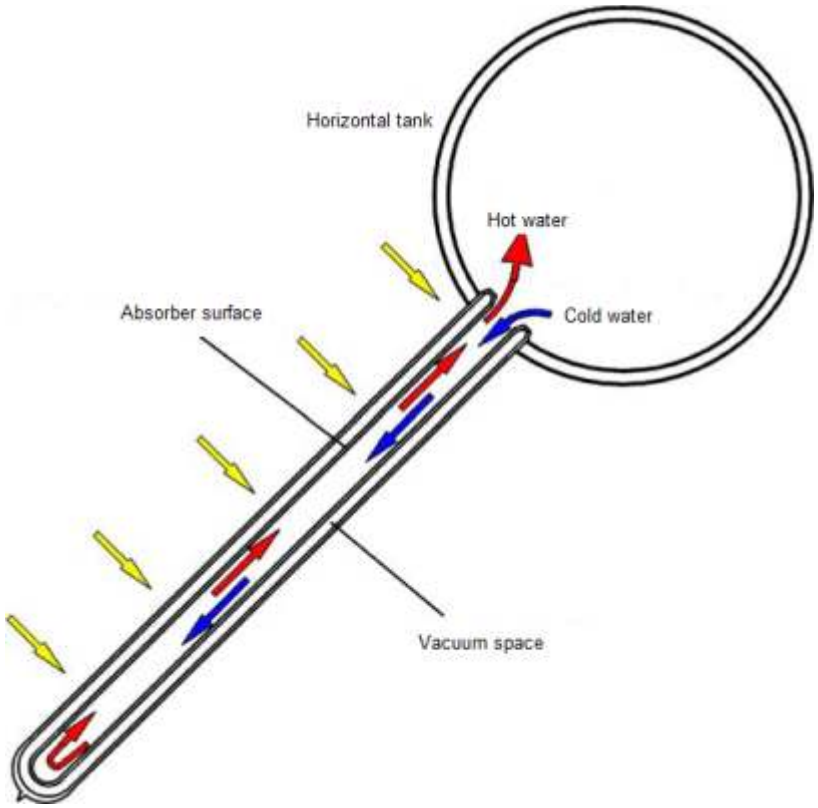


Figure. 1. Natural circulation in water-in glass solar water heater [7]

## 2. METHODOLOGY

### 2.1 Experimental Model

CFD models are widely accepted but need to be validated against experiments to gain some assurance that the calculated results would be accurate. For this study a lab-scale solar water heater was developed and used for outdoor experiments. The water heater consists of two full-scale evacuated tubes connected to a storage tank as shown in Figure 2. The tubes are 1800mm long and 58mm and 45mm external diameter and internal diameters respectively. They are inclined at $45^{o}$ to the vertical and are100mm apart. The storage tank is made of Perspex of 1mm thickness and its dimensions are 300mm x 350mm x 450mm. The top of the tank has a lid of the same material to reduce heat loss.

Figure 2. Photograph of the experimental model

A multi-channel data logger was used for recording the thermo resistor outputs at two minute time intervals during the day during the last half of May. On some days no recordings were taken as it was raining. There was no proper cover for the data logger. The thermo resistors were connected to the following points: tube inlet and outlet Centre, 165mm and 50mm above tank base, 1600mm and 750mm from the tube opening as shown in Figure 3. These points where chosen to compare temperature spatial distribution. Ambient temperature was also measured for the same period. Although temperature was recorded for the whole day only measurements between 11:30 and 12:30 where used for validating the numerical model. It was assumed that the solar radiation is almost constant during this period making it possible to derive heat flux equations for this hour.

## 2.2 Mathematical model

To investigate temperature and flow fields a 3D numerical model was developed using a Computational Fluid Dynamics (CFD) package, Fluent 6.1 to simulate the lab case. This model interprets exactly the geometry of the lab-scale experimental model so that it can be validated against experimental results. The geometry used for simulation is shown in Figure 4.

### 2.2.1 Assumptions

To model natural convection flow under study, with temperature between 0$^{o}$C and 100$^{o}$C all physical properties of water: μ, Cp, k and $\rho$ were assumed to vary with temperature as shown by the following piecewise polynomial equations from Gertzos et al [16]: For $273\ \mathrm{K} \le \mathrm{T} \le 373\ \mathrm{K}$

$$\rho = -1113.5 + 23.82T - 0.099428T^{2} + 1.8447e-4T^{3} - 1.3187e-7T^{4} \quad (1)$$

$$\mu = 0.48281 - 0.0056188T + 2.4637e-5T^2 - 4.8141e-8T^3 + 3.533e-11T^4 \quad (2)$$

$$C_p = 4.39429e4 - 4.73124e2T + 2.11109T^2 - 419028e-3T^3 + 3.125e-6T^4 \quad (3)$$

$$k = -2.74331 + 2.59806e-2T - 6.70640e-5T^2 + 5.90278e-8T^3 \quad (4)$$

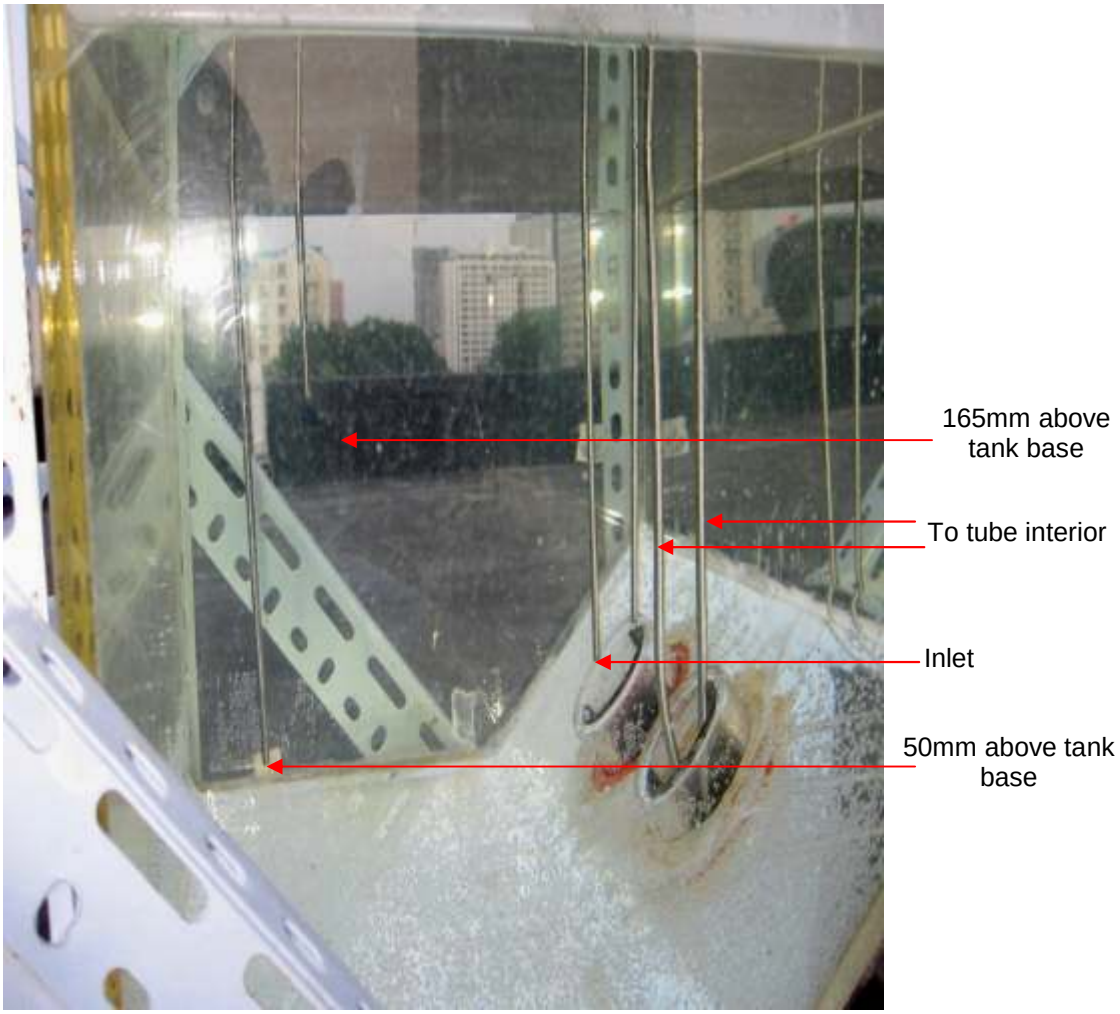


Figure 3. Temperature measuring points

It is the density difference between cold and hot water that gives rise to buoyancy force which drives the flow.

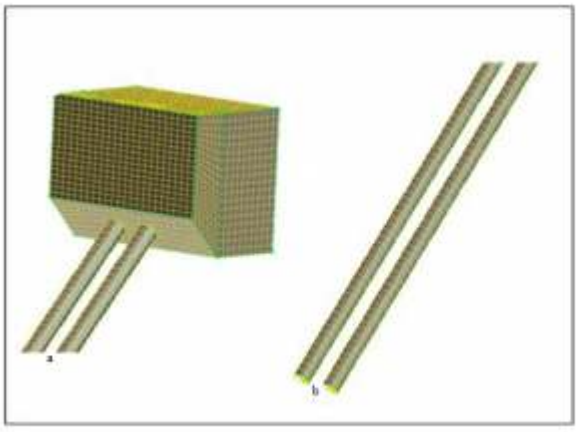

Figure 4. Computational grid: (a) the tank; (b) tubes

It was also assumed that the influence of flow and heat transfer in each tube does not significantly affect what happens in the next tube Budihardjo et al. [7]. The following forces were assumed to act on the control volume:

i. The pressure forces acting in the vertical direction on the top and bottom surfaces.
ii. The shear stresses acting in the horizontal direction on the side surfaces.
iii. The normal stresses acting on the top and bottom surfaces are small and are neglected.
iv. The force of gravity acting on the entire volume.
v. Pressure remains constant throughout the simulation.

The following assumptions were made for solar radiation:

i. The evacuated tubes can utilise solar radiation from all directions but since they are cylindrical only parts of the tube will be exposed to beam radiation depending on the solar azimuth and altitude.
ii. The intensity of solar radiation incident on each tube depends on the angle of incidence which varies with the sun's daily and seasonal movements.
iii. Each tube will cast a shadow on the adjacent tubes.

### 2.2.2 Governing equations

#### *2.2.2.1 Conservation of mass (continuity) equation*

The conservation of mass principle states that mass cannot be created or destroyed. For a steady-state flow mass inside this volume remains constant.

$$\rho\left(\frac{\partial u}{\partial x}+\frac{\partial v}{\partial y}+\frac{\partial w}{\partial z}\right)=0 \tag{5}$$

#### *2.2.2.2 Conservation of momentum equation*

Newton's second law of motion for this control volume states that the sum of forces acting on the fluid is equal to the mass of the fluid in this volume times the rate of change of its velocity (acceleration) as it moves through the volume.

$$\rho\left(u\frac{\partial u}{\partial x}+v\frac{\partial u}{\partial y}+w\frac{\partial u}{\partial z}\right)=-\frac{\partial P}{\partial x}+\mu\left(\frac{\partial^2 u}{\partial x^2}+\frac{\partial^2 u}{\partial y^2}+\frac{\partial^2 u}{\partial z^2}\right) \tag{6}$$

$$\rho\left(u\frac{\partial v}{\partial x}+v\frac{\partial v}{\partial y}+w\frac{\partial v}{\partial z}\right)=-\frac{\partial P}{\partial y}+\mu\left(\frac{\partial^2 v}{\partial x^2}+\frac{\partial^2 v}{\partial y^2}+\frac{\partial^2 v}{\partial z^2}\right) \quad (7)$$

.

$$\rho\left(u\frac{\partial w}{\partial x}+v\frac{\partial w}{\partial y}+w\frac{\partial w}{\partial z}\right)=-\frac{\partial P}{\partial z}+\mu\left(\frac{\partial^2 w}{\partial x^2}+\frac{\partial^2 w}{\partial y^2}+\frac{\partial^2 w}{\partial z^2}\right)+g\left(\rho_\infty-\rho\right) \quad (8)$$

#### *2.2.2.3 Conservation of energy equation*

The conservation of energy principle states that energy cannot be created or destroyed thus the energy content of a system is equal to the difference between energy inflow and outflow. For a steady-flow process, the net energy content of a system is constant.

$$\rho\left(u\frac{\partial T}{\partial x}+v\frac{\partial T}{\partial y}+w\frac{\partial T}{\partial z}\right)=\frac{k}{C_p}\left(\frac{\partial^2 T}{\partial x^2}+\frac{\partial^2 T}{\partial y^2}+\frac{\partial^2 T}{\partial z^2}\right) \quad (9)$$

Equations (9), (12), (13) and (21) are the governing equations for the flow under study.

### 2.2.3 Boundary conditions

The storage tank walls were modeled as a heat sink where convective boundary conditions were applied. $U_{lt}$, was assumed to be 5 W/m$^2$K on the side and bottom walls and 10 W/m$^2$K from the top wall Morrison et al [6]. Ambient temperature was assumed to be 300 K throughout the simulation. The closed ends of the tubes were assumed to be adiabatic walls with heat flux 0 W/m$^2$.

A User Defined Function (UDF) was developed for heat flux boundary conditions on the evacuated tube walls. Incident radiation passes through the outer glass tube of transmissivity, $\tau$ absorbed by the inner tube of absorptivity, $\alpha$ and converted to heat energy which is transmitted to water moving in the tube. The intensity of solar radiation incident on the tube varies with the angle of incidence, which varies according to the daily and seasonal movement sun. The relationship between the solar collector and incident radiation can be calculated using the coordinate system shown in Figure 5 and applying equations and definition given by Shah and Furbo [13], Wei et al. [15] and Duffie and Beckman [17].

The x-axis points due south, y-axis points due to the east and z-axis to the zenith. The coordinate origin is on the axial line of the absorber. L is the incident light n' is the normal of the diametric cross section of the cylindrical tube,

$$\omega=\left(\chi_s-12\right)\frac{\pi}{12} \quad (10)$$

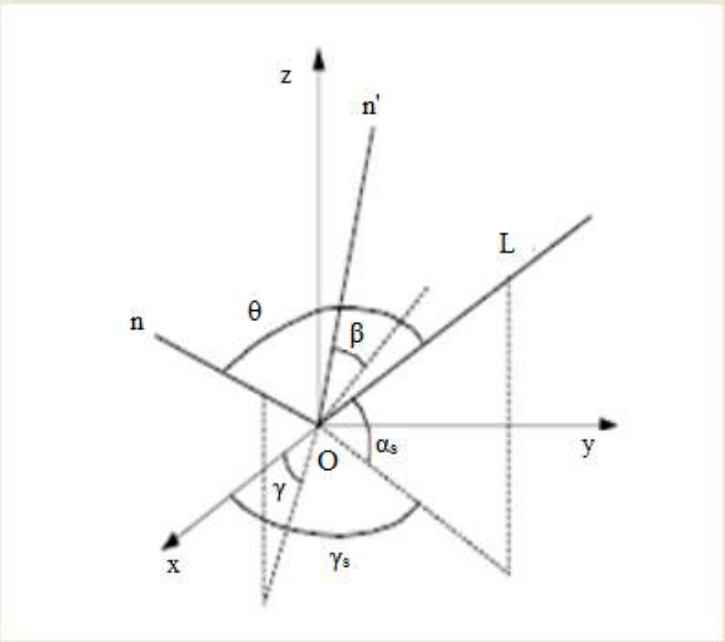


Figure 5. The coordinate system for calculating incident angle Wei et al [15]

Hour angle is the angular displacement of the sun east or west of the local meridian due to the rotation of the sun on its axis at $15^o$ per hour

Solar time, the time based on the apparent motion of the sun across the sky with solar noon the time the sun crosses the meridian of the observer. Two corrections have to be applied to standard time to convert it to solar time.

$$\chi_s = \chi_{loc} + 4\left(L_{st} - L_{loc}\right) + E \tag{11}$$

The equation of time takes into account the variations in the sun's rotational motion affecting the time the sun crosses the meridian of the observer. $E = 987\sin 2B - 7.53\cos B - 1.5\sin B$ (12)

where

$$B = \frac{360(n-81)}{364} \tag{13}$$

The declination angle, the angular position of the sun at solar noon with respect to the plane of the equator, north positive is given by

$$\delta = 23.45\sin\left(360\frac{284+n}{365}\right) \tag{14}$$

$$-23.45^o \le \delta \le 23.45^o$$

These angles can be used to calculate altitude angle and the azimuth angle of the sun in the sky for any time of the day by :

$$\sin\alpha_s = \sin\phi\sin\delta + \cos\phi\cos\delta\cos\omega \tag{15}$$

$$\cos\gamma_s = \left(\sin\alpha_s\sin\phi - \sin\delta\right)/\cos\alpha_s\cos\phi \tag{16}$$

$$\sin\gamma_s = \left(\cos\delta\sin\omega\right)/\cos\alpha_s \tag{17}$$

For a tube collector at any azimuth and tilt, the value of the cosine of $\theta$ is given by:

$$\cos\theta = \sin\delta(\cos\beta\sin\phi - \sin\beta\cos\phi\cos\gamma) + \cos\delta\cos\phi\cos\beta\cos\omega + \cos\delta\sin\phi\sin\beta\cos\gamma\cos\omega + \cos\delta\sin\beta\sin\gamma\sin\omega \quad (18)$$

The useful solar energy absorbed by the evacuated tube is calculated using equations proposed by Shah and Furbo [13] given by:

$$P_u = \int_{-\pi}^{\pi}\left(P_b + P_d + p_{gr} - P_{loss}\right)d\gamma \quad (19)$$

### 2.2.4 Heat energy loss, $P_{loss}$

$$P_{loss} = \int_{-\pi}^{\pi} A_a U_L\left(T_{fm} - T_a\right)d\gamma$$

$$= \int_{-\pi}^{\pi} L_p r_P U_L\left(T_{fm} - T_a\right)d\gamma$$

$$= 2\pi L_p r_P U_L\left(T_{fm} - T_a\right)$$

Heat loss per unit area of the tube is thus given by:

$$P_L = U_L\left(T_{fm} - T_a\right) \quad (20)$$

### 2.2.5 Power from beam radiation $P_b$

The area of the tube exposed to solar beam radiation is affected by the solar azimuth and altitude.

$$P_b = \int_{\gamma start}^{\gamma stop} F'\left(\tau\alpha\right)_e G_b A_b K_\theta R_b\, d\gamma$$

$$= F'\left(\tau\alpha\right)_e G_b L_p r_p \int_{\gamma start}^{\gamma stop} K_\theta R_b\, d\gamma$$

$$= F'\left(\tau\alpha\right)_e G_b L_p r_p K_\theta R_b\left(\gamma_{stop} - \gamma_{start}\right)$$

Heat flux through the wall of the tube is calculated from:

$$P_{Hb} = F'\left(\tau\alpha\right)_e G_b K_\theta R_b \quad (21)$$

$$K_\theta = 1 - \tan\left(\frac{\theta}{2}\right)^a,\ R_b = \frac{\cos\theta}{\cos\theta_z} \text{ and } \cos\theta_z = \cos\delta\cos\phi\cos\omega + \sin\delta\sin\phi \quad (22)$$

Beam radiation, the energy received from the sun without having been scattered by the atmosphere is calculated by assuming a clear sky.

$$G_b = G_{on}\tau_b\cos\theta_z \quad G_{on} = 1353\left(1 + 0.033\cos\left(\frac{360n}{365}\right)\right)$$

The atmospheric transmittance for beam radiation is given by

$$\tau_b = a_0 + a_1 e^{-k/\cos\theta_z} \quad (23)$$

The constants $a_0$, $a_1$ and $k$ for a standard atmosphere with a 25km visibility are calculated from the constants $a^*_0$, $a^*_1$ and $k^*$ that are given for altitudes less than 2.5 km.

$a^*_0 = 0.4237 - 0.00821(6-A)^2$, $a^*_1 = 0.5055 + 0.00595(6.5-A)^2$ and

$$k^* = 0.2711 + 0.01858(2.5 - A)^2$$

The following correction factors are applied to equation (15) to allow for different climatic conditions:

$$r_0 \equiv a_0 / a^*_0 , \quad r_1 \equiv a_1 / a^*_1 \text{ and } r_k \equiv k / k^*$$

### 2.2.6 Power from diffuse radiation $p_d$

$$P_d = \int_{-\pi}^{\pi} A_a F'(\tau\alpha)_e K_{\theta,d} F_{c-s} G_d \, d\gamma$$

$$= 2\pi r_p L_p F'(\tau\alpha)_e K_{\theta,d} G_d \int F_{c-s} d\gamma$$

$$= 2\pi r_p L_p F'(\tau\alpha)_e K_{\theta,d} G_d F_{c-s}$$

Heat flux due to diffuse radiation per unit area is thus given by

$$P_{Hd} = F'(\tau\alpha)_e K_{\theta,d} G_d F_{c-s} \quad (24)$$

$$F_{c-s} = F^*_{c-s} - F_{1-2} = 0.5 - F_{1-2} \quad (25)$$

For simplicity it was assumed that $F^*_{c-s} = F^*_{c-g} = 0.5$

$$F_{1-2} = \frac{1}{2\pi r_p}\left[(\pi - x_1 - x_3) r_p + z + (x_3 - x_1) - C\sin(x_3)\right] \quad (26)$$

$$x_1 = a\cos\left(\frac{r_c - r_p}{C}\right) \quad x_3 = a\cos\left(\frac{r_c + r_p}{C}\right) \quad (27)$$

$$Z = \sqrt{\left(C + r_c\cos(\pi + x_1) - r_p\cos(x_1)\right)^2 + \left(r_c\sin(\pi + x_1) - r_p\sin(x_1)\right)^2} \quad (28)$$

Transmission coefficient for diffuse radiation is related to that for beam radiation by:

$$\tau_d = 0.2710 - 0.2939\tau_b \ .$$

Diffuse radiation, the energy received from the sun after its radiation has been changed by scattering by the atmosphere is given by:

$$G_d = \tau_d G_{on} \quad (29)$$

$$K_{\theta,d} = K_{\theta,gr} = 1 - \tan\left(\frac{\pi}{6}\right)^a$$

### 2.2.7 Power from ground reflected radiation on the collector tube $P_{gr}$

$$P_{gr} = \int_{-\pi}^{\pi} A_a F'(\tau\alpha)_e K_{\theta,gr} F_{c-g} G_{gr} \, d\gamma$$

$$= 2\pi r_p L_p F'(\tau\alpha)_e K_{\theta,gr} G_{gr} \int F_{c-g} d\gamma$$

$$= 2\pi r_p L_p F'(\tau\alpha)_e K_{\theta,gr} G_{gr} F_{c-g}$$

Heat flux due to ground reflected radiation is given by

$$P_{Hgr} = F'(\tau\alpha)_e K_{\theta,gr} G_{gr} F_{c-g} \quad (30)$$

$$F_{c-g} = 0.5 - F_{1-2}$$

$$G_{gr} = \rho_{gr}(G_b + G_d) \quad (31)$$

The tube surface was divided into two and different boundary conditions were imposed on them. The upper part of the tube received beam and diffuse radiation while the lower part received reflected radiation. Heat loss coefficient on the tube walls was assumed to be 0.9W/m$^2$K.

Total useful heat passed on to water from the absorber tubes will be obtained by applying the following boundary equation on the tube side walls:

$$P_u = rpLG - 2\pi LrU_L(T_{fm} - T_a)\Delta t$$

## 3. RESULTS AND DISCUSSION

### 3.1 Experimental results

Figure 6 shows highest, medium and lowest measured ambient temperature for the two week period that was studied. On any particular day ambient temperature constantly fluctuated. Although the temperature was increasing (compared with the previous month), the change was not constant as shown with May 20 having higher ambient temperature than 21. This shows that the daily weather conditions are difficult to predict to high degree of accuracy basing on literature.

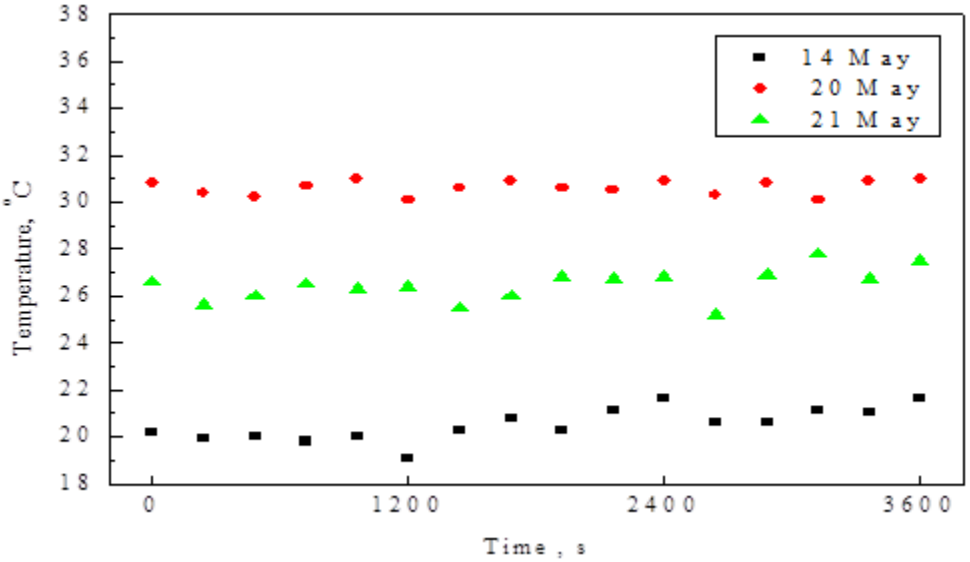


Figure 6. Ambient temperature: from 11:30 am to 12:30 pm for three days

Figure 7 shows temperature measured at two different points in the system for the three days. It was observed that there is a correlation between ambient temperature and the output temperature of the solar water. Other environmental parameters such as wind speed also have a great contribution to final output water temperature.

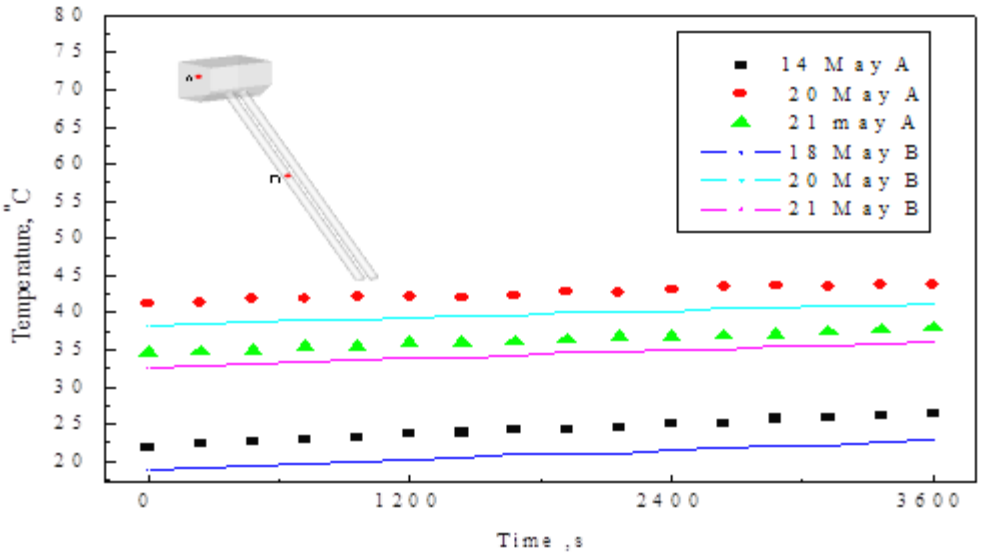


Figure 7. Temperature comparison: points inside the solar water heater for the three days

## 3.2 Numerical simulation results

Figures 8 and 9 show temperature distribution and velocity vectors in the numerical domain.

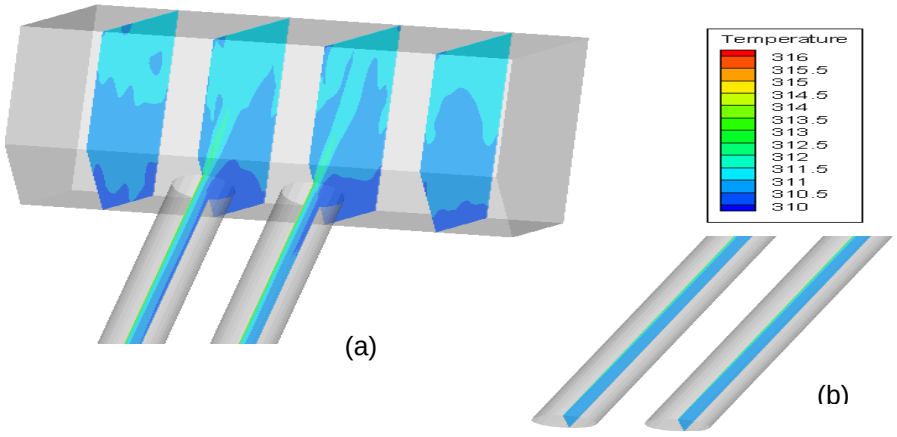


Figure 8. Temperature distribution: (a) main part of the system; (b) near tubes closed end

The flow in the tubes is bi-filamental, consisting of two main streams moving in opposing directions. On absorbing heat energy, the water becomes less dense and moves up to the tank at higher velocity where it displaces cold, less dense water that descends at lower velocity through the lower part of the tube. In the tank cold water occupies the lower part while hot water is on the top.

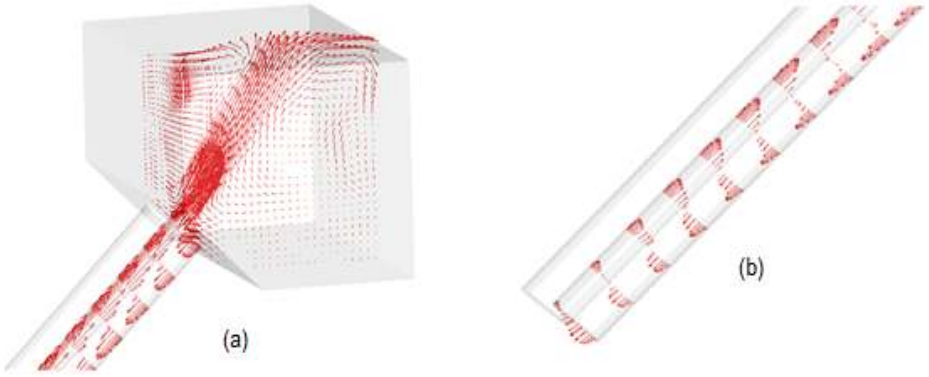


Figure 9. Velocity vectors: (a) tank (b) tube

Inside the tube, water temperature increases as it moves from the closed end up towards the tank as shown in Figure 10.

Figure

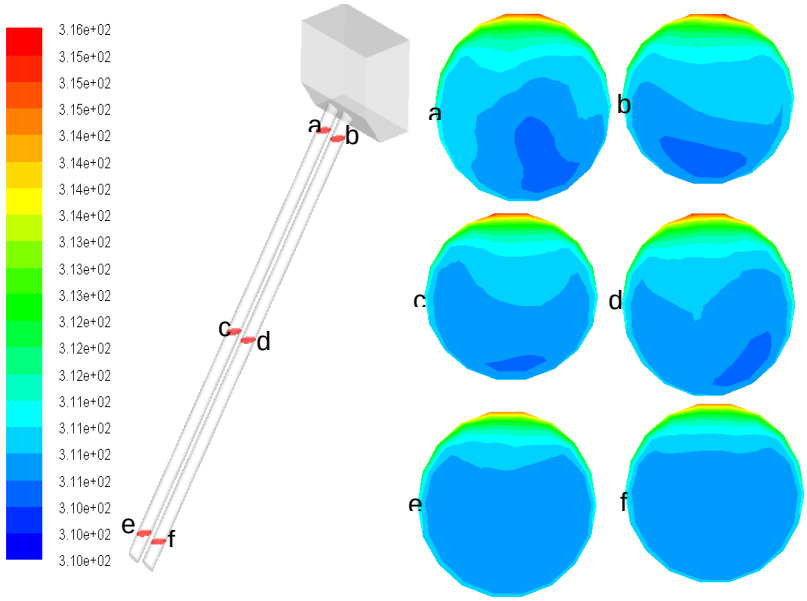


Figure 10. Temperature contours at different axial positions in the tubes

Water near the tube closed end is at low temperature and moves very slowly (Figure 11) and flow velocity increases with increasing temperature.

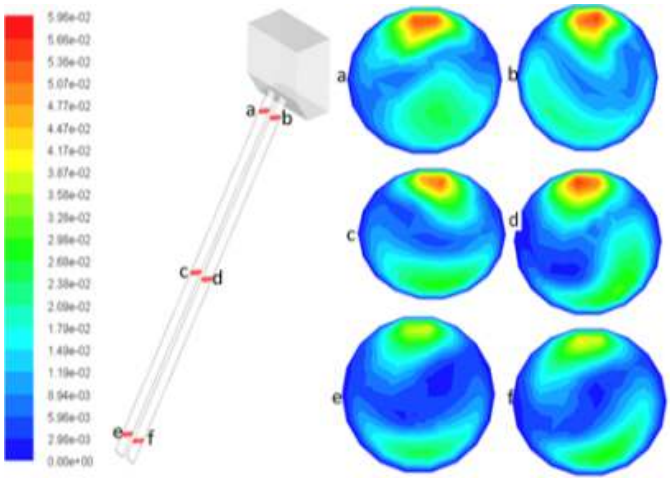


Figure11. Velocity contours at different axial positions in the tubes.

### 3.3 Numerical model validation

Figure 12 shows a comparison of numerical and experimental results. The experimental results points are scattered above and below the simulation line, which shows that the simulation is a good approximation of the experimental work.

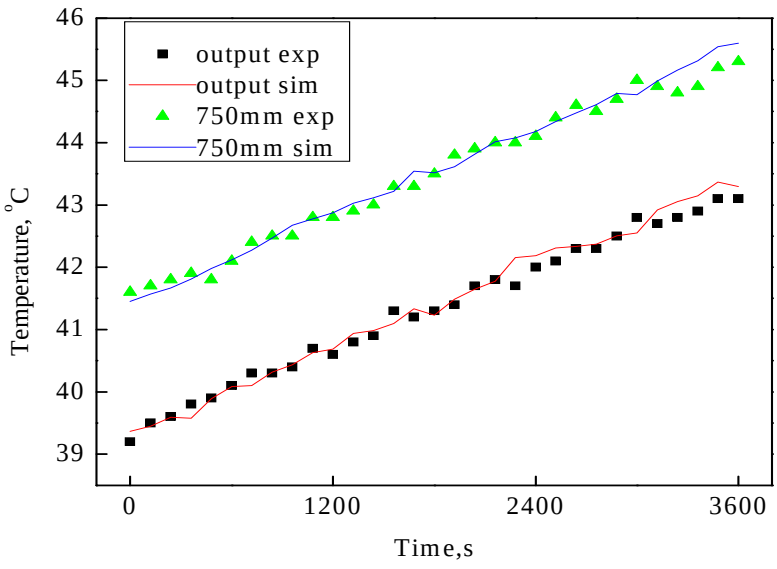


Figure12. Comparison: measured and calculated temperature at two points

According to Morrison et al. [6] errors need to be taken into account when comparing experimental and simulation results. Numerical errors can arise from inaccurate representation of boundary conditions, use of inappropriate equations and assumptions when developing the UDF and computational errors. Experimental errors can be as result of difficulties in maintaining the position of the thermo resistors and their poor calibration. Figure 13 shows a flow structure in the tank, which is not very good. Water is supposed to move from the tube opening straight upwards, not at an angle as in the diagram (b). Further investigation will be done on this issue.

However, it was noticed that for the one hour period in question, temperature rose by almost 4$^{o}$C for both models at each position. Numerical and measured values were very close at most of the compared points as shown in Figure 12. There was a good agreement in temperature stratification in the system. Both models show similar order of temperature distribution at the compared points starting from highest to lowest: point 750 mm inside the tube, outlet, 165mm above tank base, inlet, 50 mm above tank base and1600 mm inside the tube.

Experimental results by past researchers Behnia et al [2], Morrison et al [6], and Budihardjo [7] have shown that flow in the evacuated tube is bi-filamental and this has also been shown by the numerical model (Figure 13). They also observed the formation of a stagnant region near the tube closed end at low temperatures which is also predicted by this model (Figure 11c).

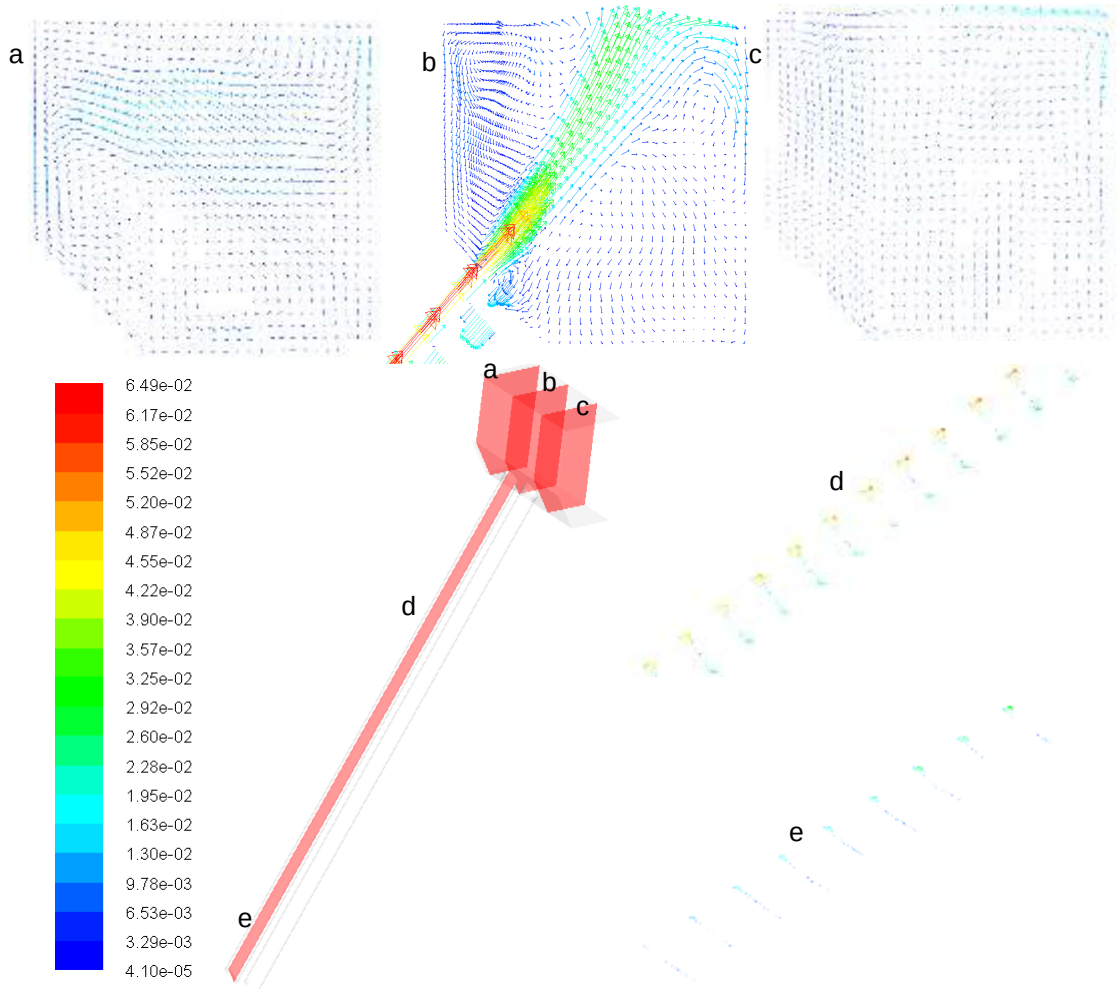

Figure 13. Flow structure inside the system: (a, b, c) different positions inside the tank; (d) tube.

All these observations validate the numerical model and give the confidence that the numerical calculations are close approximations of the real solar system output.

## 4. CONCLUSIONS

This paper concentrated on the measurement of spatial and temporal temperature distribution in a water-in-glass evacuated solar water heater. Spatial temperature distribution and its rate of change is of great importance as it influences the circulation flow rate through the tubes. A higher rate of temperature change leads to higher operational temperature which reduces water viscosity and increases density gradient. Since, it is this density gradient that drives the natural circulation, flow rate increase leading to higher system efficiency.

The computational model was validated against experimental measurements. It was observed that there is a correlation between ambient temperature and the output temperature of the solar water.The flow in the tubes is bi-filamental, consisting of two main streams moving in opposing directions. The numerical and measured values were very close at most of the compared points along the tube.Thus this model is to be used for further studies and optimisation of operational parameters of the collector system. Seasonal variation of rate of temperature change can be obtained using this model. Results obtained from further studies can be used to design a new system that works well throughout the whole year.

This model is unique in that it calculates the output temperature of service water under varying geometrical parameters at the same time taking into account the location and orientation of the collector and the daily and seasonal movement of the sun. These affect the amount of radiation that strikes on the evacuated tube surface which is then converted to heat energy.

## REFERENCES


1. Martin, B.W., 1953. Heat transfer by free convection in an open thermosyphon tube. Brit. J. Appl. Phys. 5, 91-95.
2. Behnia, M., Morrison, G.L., An experimental investigation of inclined open thermosyphons. Solar Energy 47, 313-326.
3. Gaa, F.O., Behnia, M., Morrison, G.L., 1996. Experimental study of flow rates through inclined thermosyphons. Solar Energy 57 (5), 401-408.
4. Cabanillas, R.E., Estrada, C.A., Avila, F., 1995. A device for measuring the angular distribution of incident radiation on tubular solar collectors. Renewable Energy 6 (7), 843–847.
5. Morrison, G.L, Budihardjo, I., Behnia, M., 2004. Water-in-glass evacuated tube solar water heater. Solar Energy 76, 135-140.
6. Morrison, G.L., Budihardjo, I., Behnia, M., 2005.Measurement and simulation of flow rate in a water-in-glass evacuated tube solar water heater. Solar Energy 78, 257–267.
7. Budihardjo, I., Morrison, G.L., Behnia, M., 2007. Natural circulation flow through water-in-glass evacuated tube solar collectors. Solar Energy 81, 1460–1472.
8. Budihardjo, I., Morrison, G.L., Behnia, M. development of TRNSYS models for predicting the performance of water-in-glass evacuated tube solar heaters in Australia. School of Mechanical and manufacturing Engineering, The University of New South Wales.
9. Budihardjo, I., Morrison, G.L., 2008. Performance of water-in-glass evacuated tube solar water heater. Solar Energy.
10. Kim, J. T., Ahn, H. T., Han, H., Kim, H.T., Chun, W., 2007. The performance simulation of all-glass vacuum tubes with coaxial fluid conduit. International Communications in heat and Mass Transfer 34, 587-597.

11. Han, H., Kim, J. T., Ahn, H. T., Lee, S.J., 2008. A three-dimensional performance analysis of all-glass vacuum tubes with coaxial fluid conduit. International Communications in heat and Mass Transfer 35, 589-596.
12. Kim, Y. and Seo, T., 2007. Thermal performances comparisons of the glass evacuated tube solar collectors with shapes of absorber tube. Renewable Energy 32, 772-795.
13. Shah L.J. and Furbo, S., 2004. Vertical evacuated tubular collectors utilizing solar energy from all directions. Applied Energy 78, 371-395.
14. Shah L.J. and Furbo, S., 2007. Theoretical flow investigations on an all-glass evacuated tubular collector. Solar Energy 81, 822-828.
15. Wei, S.X., Li, M., Zhou, X. Z., 2007. A theoretical study on the area compensation of non-directly-south-facing solar collectors. Applied Thermal Engineering 27, 442-449.
16. Gertzos, K.P. Pnevmatikakis, S.E. Caouris, Y.G., 2008. Experimental and numerical study of heat transfer phenomena, inside a flat-plate integrated collector storage solar water heater (ICSSWH), with indirect heat withdrawal. Energy Conversion and Management 49, 3104–3115.
17. Duffie, J.A., Beckman, W.A., 1991. Solar Engineering of Thermal Processes, Wiley-Interscience, New York.

# Nomenclature

| | |
|---|---|
| $\gamma_s$ | Sun azimuth angle [rad] |
| $\gamma$ | Tube surface azimuth angle [rad] |
| $\beta$ | Tilt angle of the evacuated tube collector [rad] |
| $\theta$ | Angle of incidence [rad] |
| $\omega$ | Hour angle [rad] |
| $\delta$ | Declination of the sun [rad] |
| $\phi$ | Local latitude [rad] |
| $\gamma_{start}$ | Start angle for tube part exposed to radiation [rad] |
| $\gamma_{stop}$ | Stop angle for tube part exposed to radiation [rad] |
| $L_{st}$ | Standard meridian for local time [rad] |
| $L_{loc}$ | Local meridian [rad] |
| $E$ | Equation of time |
| $n$ | Day of the year [-] |
| $\chi_s$ | Solar time [min] |
| $\chi_{loc}$ | Standard (local time) time [min] |
| $t_f$ | Start time [min] |
| $t_i$ | End time [min] |
| $L_p$ | Length of evacuated tube [m] |
| $r_p$ | Absorber radius [m] |
| $r_c$ | Outer glass tube radius [m] |
| $U_L$ | Tube heat loss coefficient [$Wm^{-2}K^{-1}$] |
| $U_{lt}$ | Tank heat loss coefficient [$Wm^{-2}K^{-1}$] |

| | | |
|---|---|---|
| 586 | $T_a$ | Ambient temperature [K] |
| 587 | $C$ | Tube centre distance [m] |
| 588 | $F'$ | Tube collector efficiency factor [-] |
| 589 | $(\tau\alpha)_e$ | Effective transmittance-absorptance product [-] |
| 590 | $a$ | Incident angle modifier constant [-] |
| 591 | $r_0$ | Correction factor for climate type [-] |
| 592 | $r_1$ | Correction factor for climate type [-] |
| 593 | $r_k$ | Correction factor for climate type [-] |
| 594 | $A$ | Altitude of the observer in [km] |
| 595 | $\rho_g$ | Ground albedo [-] |
| 596 | $P_L$ | Energy loss per unit area [$Wm^{-2}$] |
| 597 | $G_{on}$ | Extraterrestrial radiation[$Wm^{-2}$] |
| 598 | $G_b$ | Beam radiation [$Wm^{-2}$] |
| 599 | $P_b$ | Power from beam radiation [W] |
| 600 | $P_{Hb}$ | Heat flux from beam radiation [$Wm^{-2}$] |
| 601 | $G_d$ | Diffuse radiation[$Wm^{-2}$] |
| 602 | $K_\theta$ | Incident angle modifier for beam radiation [–] |
| 603 | $R_b$ | Geometric factor [–] |
| 604 | $\tau_b$ | Atmospheric transmittance for beam radiation |
| 605 | $P_d$ | Power from beam radiation [W] |
| 606 | $P_{Hd}$ | Heat flux from diffuse radiation [$Wm^{-2}$] |
| 607 | $G_{gr}$ | Reflected radiation [Wm-2] |
| 608 | $P_{gr}$ | Power from reflected radiation [W] |
| 609 | $P_{Hgr}$ | Heat flux from reflected radiation [$Wm^{-2}$] |
| 610 | $\tau_d$ | Transmission coefficient for diffuse radiation [-] |
| 611 | $K_{\theta,d}$ | Incident angle modifier for diffuse radiation [–] |
| 612 | $K_{\theta,gr}$ | Incident angle modifier for ground reflected radiation [–] |
| 613 | $\tau$ | Transmissivity [-] |
| 614 | $\alpha$ | Absorptivity [-] |
| 615 | $\rho$ | Density [$kgm^{-3}$] |
| 616 | $C_p$ | Constant pressure specific heat capacity [$Jkg^{-1}k^{-1}$] |
| 617 | $\mu$ | Dynamic viscosity [kg $m^{-1}s^{-1}$] |
| 618 | $k$ | Thermal conductivity [$Wm^{-1}K^{-1}$] |
| 619 | $u, v, w$ | x, y, z components of velocity |

| | | |
|---|---|---|
| $\chi_1$ | Help angle [rad] |
| $\chi_2$ | Help angle [rad] |
| $\chi_3$ | Help angle [rad] |
| $z$ | Help length [m] |
| $F_{1-2}$ | View factor from tube 1 to tube 2 [–] |
| $F_{c-g}$ | View factor from tube to ground [–] |
| $F_{c-s}$ | View factor from tube to sky [–] |